FREE CONVECTION IN WAVY POROUS ENCLOSURES WITH NON-UNIFORM TEMPERATURE BOUNDARY CONDITIONS FILLED WITH A NANOFLUID: BUONGIORNO'S MATHEMATICAL MODEL

Mikhail A. Sheremet[1,2*], Ioan Pop[3]

[1]Department of Theoretical Mechanics, Tomsk State University, 634050, Tomsk, Russia
[2]Institute of Power Engineering, Tomsk Polytechnic University, 634050, Tomsk, Russia
[3]Department of Applied Mathematics, Babeş-Bolyai University, CP 253, 400082 Cluj-Napoca, Romania
[*]Corresponding author e-mail: michael-sher@yandex.ru

In the present work, the influence of the amplitude ratio, phase deviation and undulation number on natural convection in a wavy-walled enclosures differentially heated and filled with a water based nanofluid is studied. The upper and bottom walls are wavy with several undulations. The sinusoidal distribution of temperature is imposed at the vertical walls. The flow, heat and mass transfer are calculated by solving governing equations for embody the conservation of total mass, momentum, thermal energy, and nanoparticles, taking into account the Darcy–Boussinesq–Buongiorno approximation with second order finite difference method in «stream function–temperature–concentration» formulation. Results are presented in the form of streamlines, isotherm and isoconcentration contours, and distributions of the average Nusselt number for the different values of the amplitude ratio of the sinusoidal temperature on the right side wall to that on the left side wall (γ = 0–1), phase deviation (φ = 0–π) and undulation number (κ = 1–4). It has been found that variations of the undulation number allow to control the heat and mass transfer rates. Moreover an increase in the undulation number leads to an extension of the non-homogeneous zones.

Key words: *Free convection, Wavy-walled cavity, Sinusoidal temperature, Porous media, Nanofluids, Numerical method.*

1. Introduction

Wavy geometries are used in many engineering systems as a means of enhancing the transport performance. Therefore, knowledge about flow and heat transfer through wavy surfaces becomes important in this context. Solar collectors, condensers in refrigerators, cavity wall insulating systems, grain storage containers, industrial heat radiators, for example, are a few of many applications where wavy surfaces are encountered to transfer small or large scale heat [1, 2]. The focus on the area of flow and heat transfer past wavy surfaces in complex enclosures like square, trapezoidal and rectangular has been intensifying over the years due to the increasing interest of researchers from applied

mathematics, mechanical and chemical engineering as well as from biomechanics and engineering mechanics. A great number of technical papers have been published on this subject and these have been scattered in a number of different journals. Topics range from a variety of flow situations to the use of different mathematical techniques for the analyses of complex flow situations involving wavy surfaces. Conventional heat transfer liquids have low thermal conductivity. It seems that Choi [3] was the first who introduced the term "nanofluid". A significant feature of nanofluids is thermal conductivity enhancement, a phenomenon which was first reported by Masuda et al. [4]. Many modern industries deal with heat transfer in some or the other way, and thus have a strong need for improved heat transfer media. This could possibly be nanofluids, because of some potential benefits over normal fluids – large surface area provided by nanoparticles for heat exchange, reduced pumping power due to enhanced heat transfer, minimal clogging, innovation of miniaturized systems leading to savings of energy and cost. Buongiorno [5] in his study ignored suspension, dispersion, turbulence and particle rotation, attributed by some, as the possible cause for the observed enhancement. He suggested a new model based on the mechanics of nanoparticles/basefluid relative velocity. Buongiorno [5] took the absolute velocity of nanoparticles as the sum of the base-fluid velocity and a relative velocity, (which he calls a slip velocity). He considered seven slip mechanisms such as inertia, Brownian diffusion, thermophoresis, diffusophoresis, Magnus effects, fluid drainage and gravity settling. He studied each one of these and concluded that in the absence of turbulent effects, Brownian diffusion and thermophoresis are the dominated mechanisms. Based on these two effects, he derived the conservation equations.

Convection in porous media is of practical applications in modern science and engineering, including food and chemical processes, rotating machineries like nuclear reactors, petroleum industry, biomechanics, geophysical problems, food, etc. The fundamental nature and the growing volume of work in this area are amply documented in the books by Nield and Bejan [6], Ingham and Pop [7], Vafai [8], Pop and Ingham [9].

Because of their unique properties as heat transfer fluids, nanofluids are being looked upon as great coolants of the future. Thus studies need to be conducted involving nanofluids in porous media and without it [10–14]. Vadasz [15] has proposed thermal lagging between the particle and fluid phases as an explanation for the observed increase in the thermal conductivity of nanofluids. Due to applications of nanofluids and porous media theory in drying, freezing of foods, and applications in everyday technology such as microwave heating, rapid heat transfer from computer chips via use of porous metal foams and their use in heat pipes, studies of convection in wavy porous enclosures turns important. By our best of knowledge no other study on the present problem is available. Therefore we intend to investigate this problem further. It should be noted that the present paper is a continuation of an investigation concerning sinusoidal temperature distributions presented in [16] and wavy wall influence presented in [17]. Here our particular efforts have been focused on the effects of the amplitude ratio of the sinusoidal temperature, phase deviation and undulation number of horizontal walls on the fluid flow, heat and mass transfer characteristics.

2. Basic equations

Consider the natural convection in a wavy-walled porous enclosure filled with a water based nanofluid. It is assumed that nanoparticles are suspended in the nanofluid using either surfactant or

surface charge technology. This prevents nanoparticles from agglomeration and deposition on the porous matrix [18]. A schematic geometry of the problem under investigation is shown in fig. 1. The cavity is assumed to be impermeable and the wavy walls are considered to be thermally insulated. At the same time the vertical walls have sinusiodal temperature distributions according to the space coordinate [16, 17, 19]. It should be noted that the upper and the bottom wavy walls of the cavity are described by the special relations [17, 20] for $\bar{y}_1$, $\bar{y}_2$, $\bar{\Delta}$ (see Nomenclature).

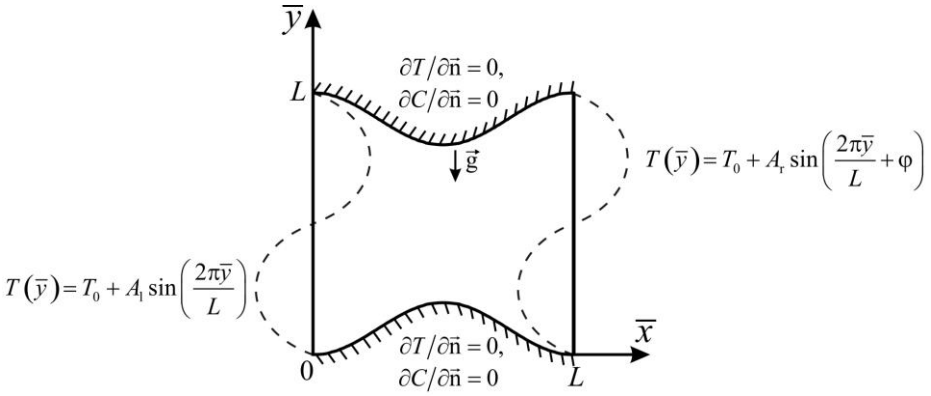

Fig. 1. Physical model and coordinate system

The Darcy–Boussinesq model is used. Homogeneity and local thermal equilibrium in the porous medium is considered. The flow is assumed to be slow so that an advective term and a Forchheimer quadratic term do not appear in the momentum equation. Taking into account these assumptions the partial differential equations have been formulated in terms of the dimensionless stream function, temperature and concentration variables [16, 17]

$$\frac{\partial^2\psi}{\partial x^2} + \frac{\partial^2\psi}{\partial y^2} = -\mathrm{Ra}\frac{\partial\theta}{\partial x} + \mathrm{Ra}\cdot\mathrm{Nr}\frac{\partial\phi}{\partial x} \tag{1}$$

$$\frac{\partial\psi}{\partial y}\frac{\partial\theta}{\partial x} - \frac{\partial\psi}{\partial x}\frac{\partial\theta}{\partial y} = \frac{\partial^2\theta}{\partial x^2} + \frac{\partial^2\theta}{\partial y^2} + \mathrm{Nb}\left(\frac{\partial\phi}{\partial x}\frac{\partial\theta}{\partial x} + \frac{\partial\phi}{\partial y}\frac{\partial\theta}{\partial y}\right) + \mathrm{Nt}\left[\left(\frac{\partial\theta}{\partial x}\right)^2 + \left(\frac{\partial\theta}{\partial y}\right)^2\right] \tag{2}$$

$$\frac{\partial\psi}{\partial y}\frac{\partial\phi}{\partial x} - \frac{\partial\psi}{\partial x}\frac{\partial\phi}{\partial y} = \frac{1}{\mathrm{Le}}\left[\frac{\partial^2\phi}{\partial x^2} + \frac{\partial^2\phi}{\partial y^2}\right] + \frac{1}{\mathrm{Le}}\frac{\mathrm{Nt}}{\mathrm{Nb}}\left[\frac{\partial^2\theta}{\partial x^2} + \frac{\partial^2\theta}{\partial y^2}\right] \tag{3}$$

The corresponding boundary conditions for these equations are given by

$$\begin{aligned}
&\psi = 0, \quad \theta = \sin(2\pi y), \quad \mathrm{Nb}\frac{\partial\phi}{\partial x} + \mathrm{Nt}\frac{\partial\theta}{\partial x} = 0 \quad \text{on} \quad x = 0 \\
&\psi = 0, \quad \theta = \gamma\sin(2\pi y + \varphi), \quad \mathrm{Nb}\frac{\partial\phi}{\partial x} + \mathrm{Nt}\frac{\partial\theta}{\partial x} = 0 \quad \text{on} \quad x = 1 \\
&\psi = 0, \quad \frac{\partial\theta}{\partial\vec{n}} = 0, \quad \frac{\partial\phi}{\partial\vec{n}} = 0 \quad \text{on} \quad y = y_1 \text{ and } y = y_2
\end{aligned} \tag{4}$$

Taking into account the dimensionless variables the upper and the bottom wavy walls of the cavity are described by the relations [17] for y_1, y_2, Δ (see Nomenclature).

The physical quantities of interest are the average Nusselt and Sherwood numbers:

$$\overline{\mathrm{Nu}_\mathrm{l}} = -\int_0^1 \left(\frac{\partial\theta}{\partial x}\right)_{x=0} \mathrm{d}y, \quad \overline{\mathrm{Sh}_\mathrm{l}} = -\int_0^1 \left(\frac{\partial\phi}{\partial x}\right)_{x=0} \mathrm{d}y, \quad \overline{\mathrm{Nu}_\mathrm{r}} = -\int_0^1 \left(\frac{\partial\theta}{\partial x}\right)_{x=1} \mathrm{d}y, \quad \overline{\mathrm{Sh}_\mathrm{r}} = -\int_0^1 \left(\frac{\partial\phi}{\partial x}\right)_{x=1} \mathrm{d}y \tag{5}$$

3 Numerical method

The enclosure in the *x* and *y* plane is modified into a rectangular cavity in the computational region using special algebraic transformation [17] by introducing new variables ξ and η. On the basis of this abovementioned transformation [17] the governing equations (1)–(4) can be rewritten as:

$$\frac{\partial^2\psi}{\partial\xi^2} + 2\frac{\partial\eta}{\partial x}\frac{\partial^2\psi}{\partial\xi\partial\eta} + \left[\left(\frac{\partial\eta}{\partial x}\right)^2 + \left(\frac{\partial\eta}{\partial y}\right)^2\right]\frac{\partial^2\psi}{\partial\eta^2} + \frac{\partial^2\eta}{\partial x^2}\frac{\partial\psi}{\partial\eta} = -\mathrm{Ra}\left(\frac{\partial\theta}{\partial\xi} + \frac{\partial\eta}{\partial x}\frac{\partial\theta}{\partial\eta}\right) + \mathrm{Ra}\cdot\mathrm{Nr}\left(\frac{\partial\phi}{\partial\xi} + \frac{\partial\eta}{\partial x}\frac{\partial\phi}{\partial\eta}\right) \tag{6}$$

$$\begin{aligned}&\frac{\partial\eta}{\partial y}\frac{\partial\psi}{\partial\eta}\frac{\partial\theta}{\partial\xi} - \frac{\partial\eta}{\partial y}\frac{\partial\psi}{\partial\xi}\frac{\partial\theta}{\partial\eta} = \frac{\partial^2\theta}{\partial\xi^2} + 2\frac{\partial\eta}{\partial x}\frac{\partial^2\theta}{\partial\xi\partial\eta} + \left[\left(\frac{\partial\eta}{\partial x}\right)^2 + \left(\frac{\partial\eta}{\partial y}\right)^2\right]\frac{\partial^2\theta}{\partial\eta^2} + \frac{\partial^2\eta}{\partial x^2}\frac{\partial\theta}{\partial\eta} + \\ &+\mathrm{Nb}\left[\left(\frac{\partial\phi}{\partial\xi} + \frac{\partial\eta}{\partial x}\frac{\partial\phi}{\partial\eta}\right)\left(\frac{\partial\theta}{\partial\xi} + \frac{\partial\eta}{\partial x}\frac{\partial\theta}{\partial\eta}\right) + \left(\frac{\partial\eta}{\partial y}\right)^2\frac{\partial\phi}{\partial\eta}\frac{\partial\theta}{\partial\eta}\right] + \mathrm{Nt}\left[\left(\frac{\partial\theta}{\partial\xi} + \frac{\partial\eta}{\partial x}\frac{\partial\theta}{\partial\eta}\right)^2 + \left(\frac{\partial\eta}{\partial y}\frac{\partial\theta}{\partial\eta}\right)^2\right]\end{aligned} \tag{7}$$

$$\begin{aligned}&\frac{\partial\eta}{\partial y}\frac{\partial\psi}{\partial\eta}\frac{\partial\phi}{\partial\xi} - \frac{\partial\eta}{\partial y}\frac{\partial\psi}{\partial\xi}\frac{\partial\phi}{\partial\eta} = \frac{1}{\mathrm{Le}}\left\{\frac{\partial^2\phi}{\partial\xi^2} + 2\frac{\partial\eta}{\partial x}\frac{\partial^2\phi}{\partial\xi\partial\eta} + \left[\left(\frac{\partial\eta}{\partial x}\right)^2 + \left(\frac{\partial\eta}{\partial y}\right)^2\right]\frac{\partial^2\phi}{\partial\eta^2} + \frac{\partial^2\eta}{\partial x^2}\frac{\partial\phi}{\partial\eta}\right\} + \\ &+\frac{1}{\mathrm{Le}}\frac{\mathrm{Nt}}{\mathrm{Nb}}\left\{\frac{\partial^2\theta}{\partial\xi^2} + 2\frac{\partial\eta}{\partial x}\frac{\partial^2\theta}{\partial\xi\partial\eta} + \left[\left(\frac{\partial\eta}{\partial x}\right)^2 + \left(\frac{\partial\eta}{\partial y}\right)^2\right]\frac{\partial^2\theta}{\partial\eta^2} + \frac{\partial^2\eta}{\partial x^2}\frac{\partial\theta}{\partial\eta}\right\}\end{aligned} \tag{8}$$

The corresponding boundary conditions of these equations are given by

$$\begin{aligned}&\psi = 0, \quad \theta = \sin(2\pi\eta), \quad \mathrm{Nb}\frac{\partial\phi}{\partial\xi} + \mathrm{Nt}\frac{\partial\theta}{\partial\xi} = 0 \quad \text{on} \quad \xi = 0\\ &\psi = 0, \quad \theta = \gamma\sin(2\pi\eta + \varphi), \quad \mathrm{Nb}\frac{\partial\phi}{\partial\xi} + \mathrm{Nt}\frac{\partial\theta}{\partial\xi} = 0 \quad \text{on} \quad \xi = 1\\ &\psi = 0, \quad \frac{\partial\theta}{\partial\eta} = 0, \quad \frac{\partial\phi}{\partial\eta} = 0 \quad \text{on} \quad \eta = 0 \text{ and } \eta = 1\end{aligned} \tag{9}$$

The partial differential equations (6)–(8) with corresponding boundary conditions (9) were solved using the finite difference method. The detailed description of the developed solution method and comprehensive verification of an in-house computational fluid dynamic code have been presented in [16, 17, 21, 22].

The performance of wavy walls part of the model was tested against the results of Oztop et al. [20] for steady-state natural convection in a wavy cavity with isothermal vertical walls filled with the regular fluid for Prandtl number 0.7. Figure 2 shows a good agreement between the obtained streamlines and isotherms for different Rayleigh numbers and the numerical data of Oztop et al. [20].

The grid independent solution for the present problem has been presented in detail in [17]. Taking into account these results the uniform grid of 300×300 points has been selected for the following analysis.

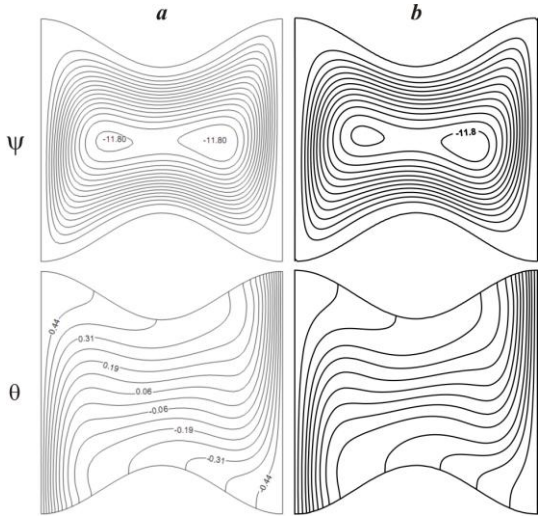

Fig. 2. Comparison of streamlines ψ and isotherms θ at $Ra_i = Ra_e = 10^5$, $a = 0.9$: numerical data of Oztop et al. [20] – *a*, present results – *b*

4 Results and discussion

Numerical investigations of the boundary value problem (6)–(9) has been carried out at the following values of key parameters: Ra = 100, Le = 100, Nr = Nb = Nt = 0.1, $a = 0.9$, the amplitude ratio of the sinusoidal temperature on the right side wall to that on the left side wall ($\gamma = 0$–1), phase deviation ($\varphi = 0$–π), undulation number ($\kappa = 1$–4). Particular efforts have been focused on the effects of these parameters on the fluid flow, heat and mass transfer characteristics.

Figure 3 illustrates streamlines, isotherms and isoconcentrations at different values of the amplitude ratio of the sinusoidal temperature on the right side wall to that on the left side wall. At $\gamma = 0$ (fig. 3*a*) when the temperature at the right vertical wall equals zero, two horizontal convective cells are formed inside the cavity. An appearance of these vortices can be explained by an effect of the periodic temperature conditions imposed upon the left vertical wall. At this regime one can find an influence of convective heat transfer mechanism on velocity and temperature fields that leads to small distortion of isotherm $\theta = 0$ close to the right wall. It should be noted that an intensity of the top convective cell is greater than an intensity of the bottom one $\left|\psi\right|_{\max}^{\text{top cell}} = 2.55 > \left|\psi\right|_{\max}^{\text{bottom cell}} = 2.4$ that can be explained by more intensive heating of the bottom part of the cavity. At the same time the distribution of nanoparticles is homogeneous because the nanoparticles volume fraction insignificantly deviates from the average value $\phi = 1$.

An increase in the amplitude ratio up to $\gamma = 0.25$ (fig. 3*b*), that characterizes a presence of small temperature differences at the right vertical wall, leads to a formation of extra weak convective cells close to the right vertical wall. Isotherms reflect a formation of both a heat source at the bottom part and a heat sink at the top part of the right vertical wall. An appearance of such heat elements leads to both a distortion of the isotherm $\theta = 0$ close to the right wall in comparison with the previous case $\gamma = 0$ (fig. 3*a*) and a formation of additional less homogeneous areas close to these heat elements. The latter can be explained by an influence of the heat conduction mechanism on temperature distributions in these zones. It is well known that heat conduction intensifies the thermophoresis effect and as a result we have less homogeneous distributions of nanoparticles. Further increase in γ leads to both an intensification of the right top and bottom convective cells and an expansion of less homogeneous areas close to the heat sink and heat source. An increase in the convective cells intensity is due to an

increase in the right wall temperature and as a result an increase in the temperature difference near this wall. It is worth noting that symmetric location of the heat sources and sinks leads to a formation of symmetric thermo-hydrodynamic structures inside the cavity at $\gamma = 1.0$ (fig. 3*e*).

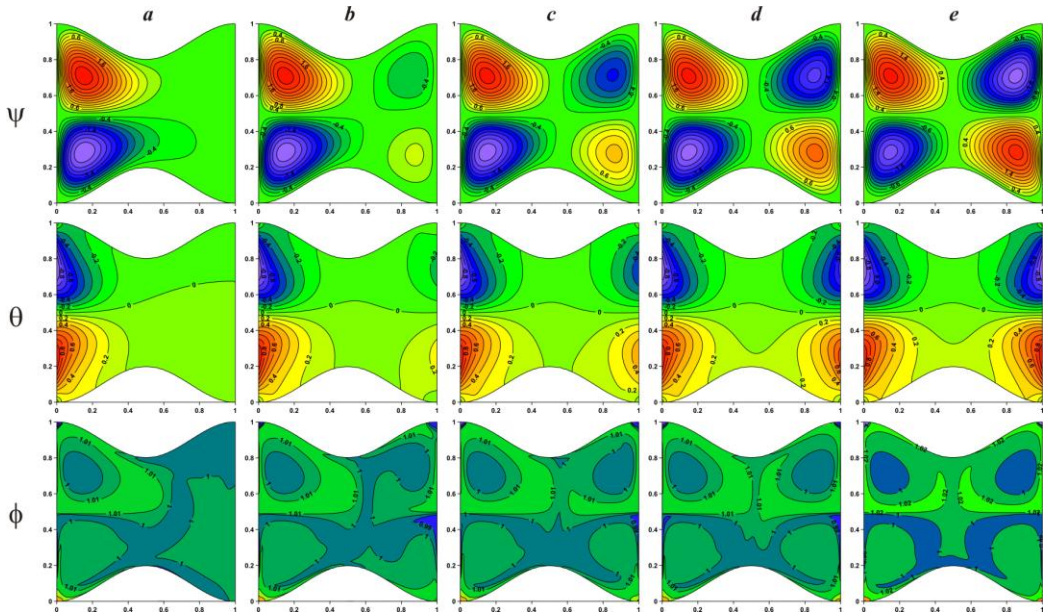

Fig. 3. Streamlines ψ, isotherms θ and isoconcentrations ϕ for φ = 0, κ = 1: γ = 0 – *a*, γ = 0.25 – *b*, γ = 0.5 – *c*, γ = 0.75 – *d*, γ = 1.0 – *e*

An effect of the dimensionless time and amplitude ratio on the average Nusselt number at left vertical wall is depictured in fig. 4. It is necessary to note that an increase in γ leads to a decrease in the average Nusselt number and, accordingly in the average Sherwood number taking into account boundary conditions (9). These changes can be explained by an interaction between thermal boundary layers and concentration boundary layers formed close to the vertical side walls having periodic temperature. Such interaction leads to a decrease in the temperature and concentration differences close to these walls owing to a reduction of convective cells and areas of temperature and concentration changes.

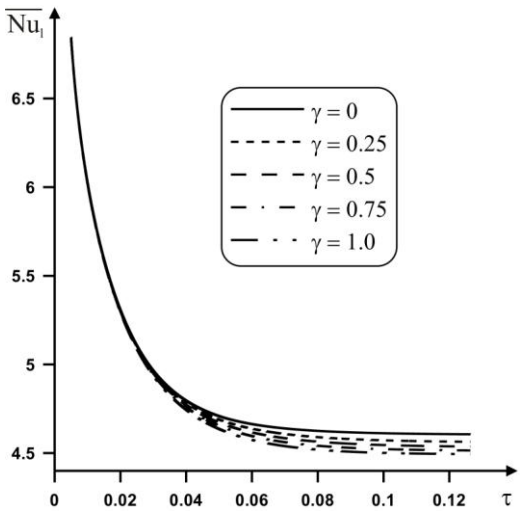

Fig. 4. Variation of the average Nusselt number at left vertical wall with the amplitude ratio and dimensionless time for φ = 0, κ = 1

Figures 3*e* and 5 illustrate streamlines, isotherms and isoconcentrations at different values of the phase deviation φ for γ = 1, κ = 1. An increase in the phase deviation up to π/4 (fig. 5*a*) leads to a combination of the left bottom clockwise convective cell and the right upper one. Such changes are caused by both a decrease in sizes of the right bottom heat source and an appearance of an extra heat source in the upper part of the right side wall. The latter leads to a formation of weak counterclockwise convective cell close to this small heat source. It should be noted that an appearance of the abovementioned heat source displays a deviation up to 5% from the average value ϕ = 1 in the upper part of the cavity close to the right vertical wall. But in general, the distribution of the nanoparticles is highly homogeneous. An increase in φ up to π/2 (fig. 5*b*) leads to both an attenuation of counterclockwise convective cell located in the left upper part of the cavity and an intensification of counterclockwise convective cell located in the right upper part of the cavity. At the same time the main clockwise vortex is intensified and deforms the convective cell located in the right bottom part of the cavity. The main reason for such hydrodynamic behaviour is the changes in position of heat sources and heat sinks on the right vertical wall. Isoconcentrations reflect an increase in sizes of the zone of the non-homogeneous distributions of nanoparticles close to the upper right corner of the cavity in comparison with the previous case φ = π/4 (fig. 5*a*). Further increase in φ leads to an attenuation of the global bottom convective cell and an intensification of the upper one and at φ = π (fig. 5*d*) one can find two horizontal vortices of equal intensities. Distributions of nanoparticles reflect structures of convective cells and characterize a formation of two large homogeneous areas.

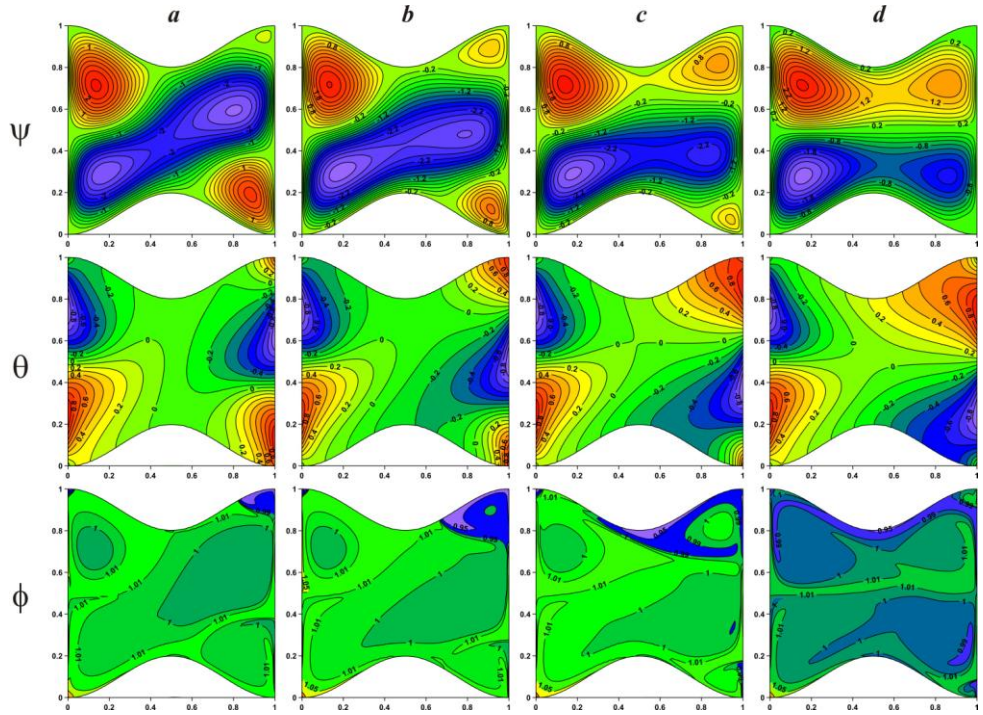

Fig. 5. Streamlines ψ, isotherms θ and isoconcentrations ϕ for γ = 1, κ = 1: φ = π/4 – *a*, φ = π/2 – *b*, φ = 3π/4 – *c*, φ = π – *d*

An effect of the dimensionless time and phase deviation on the average Nusselt number at left vertical wall is depictured in fig. 6. It should be noted that an increase in φ leads to an increase in the average Nusselt number and, accordingly in the average Sherwood number with formation of non-monotonic regions. An appearance of these increasing and decreasing zones characterizes a

replacement of several velocity and temperature configurations before steady-state regime. Such behaviour can be considered as unsteady regime.

Figures 3*e* and 7 illustrate streamlines, isotherms and isoconcentrations at different values of the undulation number κ for γ = 1, φ = 0. An increase in the undulation number leads to an attenuation of convective cells inside the cavity owing to an appearance of natural hydrodynamic obstacles in view of distortions of the top and bottom walls. At the same time the isotherms reflect insignificant changes in temperature distributions. Isoconcentrations characterize homogeneous distributions of nanoparticles inside the cavity with less homogeneous areas close to the heat elements. It is interesting to note that an increase in the undulation number leads to an expansion of the non-homogeneous zones.

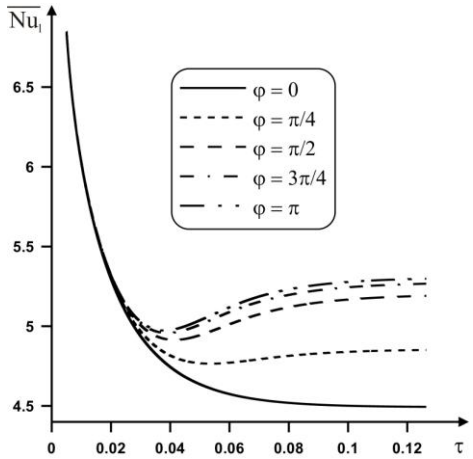

Fig. 6. Variation of the average Nusselt number at left vertical wall with the phase deviation and dimensionless time for κ = 1, γ = 1

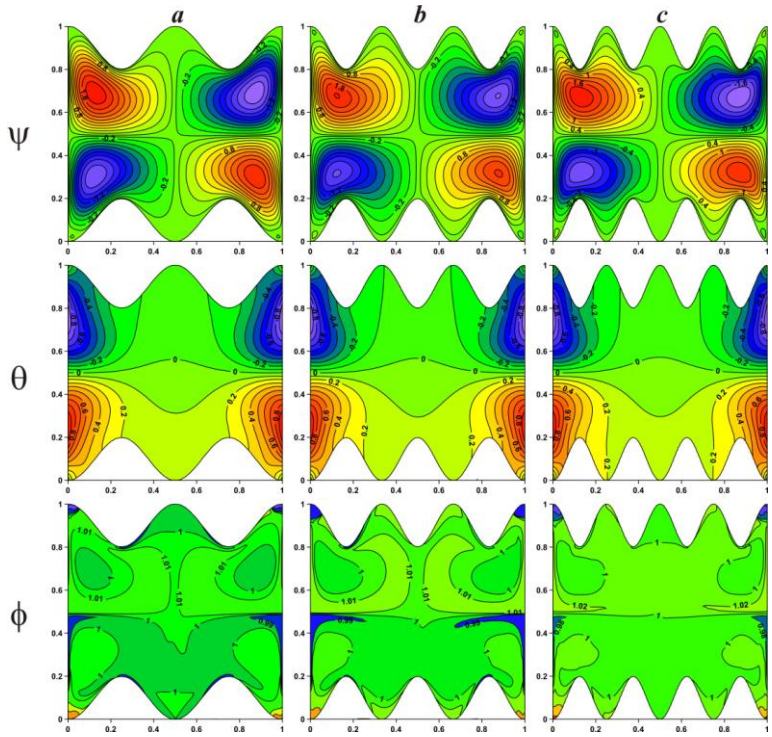

Fig. 7. Streamlines ψ, isotherms θ and isoconcentrations ϕ for γ = 1, φ = 0: κ = 2 – *a*, κ = 3 – *b*, κ = 4 – *c*

An effect of the dimensionless time and undulation number on the average Nusselt number at the left vertical wall is depictured in fig. 8. It is necessary to note that an increase in κ leads to an increase in the average Nusselt number and, accordingly in the average Sherwood number. These changes can be explained by a decrease in distance between the isothermal vertical wall and adiabatic wavy walls in the upper and bottom part that is reflected in a decrease in the thermal boundary layer thickness.

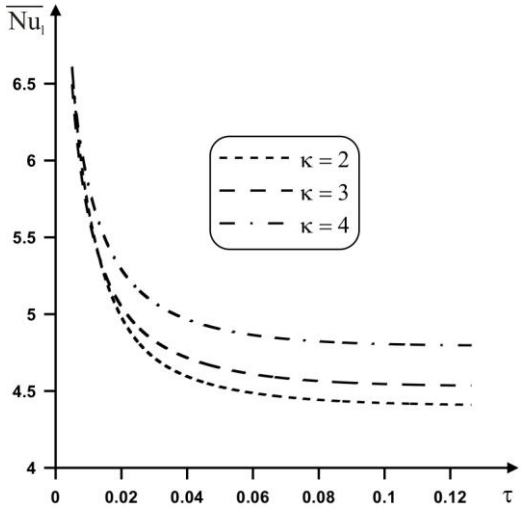

Fig. 8. Variation of the average Nusselt number at left vertical wall with the undulation number and dimensionless time for φ = 0, γ = 1

5. Conclusions

A two-dimensional porous cavity with wavy bottom and top walls having sinusoidal temperature distributions on both vertical walls and filled with a water based nanofluid has been studied. The mathematical model has been formulated in dimensionless stream function and temperature taking into account the Darcy–Boussinesq approximation and the nanofluid model proposed by Buongiorno. The governing equations have been solved numerically on the basis of a second-order accurate finite difference method. The developed algorithm has been validated by direct comparisons with previously published papers and the results have been found to be in good agreement. The results have been presented in terms of the streamlines, isotherms, isoconcentrations and average Nusselt number at left vertical wall at a wide range of key parameters. The study has indicated that the average Nusselt and Sherwood numbers are increasing functions of the phase deviation and undulation number and also decreasing functions of the amplitude ratio. The abovementioned results have indicated that it is possible to control heat and mass transfer rates during the process with help of the undulation number. It has been found also that an increase in the undulation number leads to an expansion of the non-homogeneous zones.

Acknowledgements

This work of M.A. Sheremet was conducted as a government task of the Ministry of Education and Science of the Russian Federation, Project Number 13.1919.2014/K. The authors also wish to express their thanks to the very competent Reviewers for the valuable comments and suggestions.

Nomenclature

a, b	constants that determine the shape and the contraction ratio of the wavy cavity $(a+b=1)$, [–]
A_l	amplitude of the sinusoidal profiles at the left wall, [m]
A_r	amplitude of the sinusoidal profiles at the right wall, [m]
C	nanoparticle volume fraction, [–]
C_0	reference nanoparticle volume fraction, [–]
D_B	Brownian diffusion coefficient, [$\mathrm{m^2 s^{-1}}$]
D_T	thermophoretic diffusion coefficient, [$\mathrm{m^2 s^{-1}}$]
g	gravitational acceleration, [$\mathrm{m/s^2}$]
K	permeability of the porous medium, [$\mathrm{m^2}$]
L	size of the cavity, [m]
Le	Lewis number $\left(=\alpha_\mathrm{m}/\varepsilon D_\mathrm{B}\right)$, [–]
$\vec{\mathrm{n}}$	unit normal vector to the wall, [m]
Nb	Brownian motion parameter $\left(=\delta D_\mathrm{B} C_0/\alpha_\mathrm{m}\right)$, [–]
Nr	buoyancy-ratio parameter $\left(=\left(\rho_\mathrm{p}-\rho_{\mathrm{f}0}\right)C_0 \big/ \rho_{\mathrm{f}0}\beta\Delta T\left(1-C_0\right)\right)$, [–]
Nt	thermophoresis parameter $\left(=\delta D_\mathrm{T}\Delta T/\alpha_\mathrm{m} T_0\right)$, [–]
$\overline{\mathrm{Nu_l}}$	average Nusselt number at left wall, [–]
$\overline{\mathrm{Nu_r}}$	average Nusselt number at right wall, [–]
Ra	Rayleigh number $\left(=\left(1-C_0\right)gK\rho_{\mathrm{f}0}\beta\Delta TL/\left(\alpha_\mathrm{m}\mu\right)\right)$, [–]
$\overline{\mathrm{Sh_l}}$	average Sherwood number at left wall, [–]
$\overline{\mathrm{Sh_r}}$	average Sherwood number at right wall, [–]
T	dimensional fluid temperature, [K]
T_0	reference temperature of the sinusoidal temperature profiles on the left and right side walls, [K]
$\bar{x}$	dimensional Cartesian coordinate measured along the bottom wall of the cavity, [m]
$\bar{y}$	dimensional Cartesian coordinate measured along the vertical wall of the cavity, [m]
$\bar{y}_1$	dimensional Cartesian coordinate of the bottom wavy wall $\left(=L-L\left[a+b\cos\left(2\pi\kappa\bar{x}/L\right)\right]\right)$, [m]
$\bar{y}_2$	dimensional Cartesian coordinate of the upper wavy wall $\left(=L\left[a+b\cos\left(2\pi\kappa\bar{x}/L\right)\right]\right)$, [m]
y_1	dimensionless Cartesian coordinate of the bottom wavy wall $\left(=1-a-b\cos\left(2\pi\kappa x\right)\right)$, [–]
y_2	dimensionless Cartesian coordinate of the upper wavy wall $\left(=a+b\cos\left(2\pi\kappa x\right)\right)$, [–]
x, y	dimensionless Cartesian coordinates, [–]

Greek symbols

α_m	effective thermal diffusivity of the porous medium, [$\mathrm{m^2 s^{-1}}$]
β	coefficient of thermal expansion, [$\mathrm{K^{-1}}$]

δ	parameter defined by $\left(=\varepsilon\left(\rho C_p\right)_{\mathrm{p}}/\left(\rho C_p\right)_{\mathrm{f}}\right)$, [–]
$\bar{\Delta}$	dimensional distance between the upper and bottom wavy walls $\left(=\bar{y}_2-\bar{y}_1=2L\left[a+b\cos\left(2\pi\kappa\bar{x}/L\right)\right]-L\right)$, [m]
Δ	dimensionless distance between the upper and bottom wavy walls $\left(=y_2-y_1=2a+2b\cos\left(2\pi\kappa x\right)-1\right)$, [–]
ΔT	dimensional temperature difference $\left(=A_1\right)$, [K]
μ	dynamic viscosity, [Pa·s]
θ	dimensionless temperature, [–]
$\rho_{\mathrm{f}0}$	reference density of the fluid, [kg/m^3]
ρ_{p}	nanoparticle mass density, [kg/m^3]
$\left(\rho C_p\right)_{\mathrm{f}}$	volumetric heat capacity of the base fluid, [Jm^{-3}K^{-1}]
$\left(\rho C_p\right)_{\mathrm{p}}$	effective volumetric heat capacity of the nanoparticle material, [Jm^{-3}K^{-1}]
ε	porosity of the porous medium, [–]
τ	dimensionless time, [–]
γ	amplitude ratio of the sinusoidal temperature on the right side wall to that on the left side wall $\left(=A_{\mathrm{r}}/A_{\mathrm{l}}\right)$, [–]
ξ, η	dimensionless new independent variables, [–]
φ	phase of the sinusoidal profiles at the right wall, [–]
κ	number of undulation, [–]
ϕ	rescaled nanoparticle volume fraction, [–]
$\bar{\psi}$	dimensional stream function, [m^{2}s^{-1}]
ψ	dimensionless stream function, [–]

Subscripts

f	fluid
l	left
m	medium
p	particle
r	right
0	reference value

References

[1] Sabeur-Bendehina, A., Imine, O., Adjlout, L., Laminar free convection in undulated cavity with non-uniform boundary conditions, *C. R. Mecanique*, *339* (2011), 1, pp. 42-57.

[2] Khanafer, K., Al-Azmi, B., Marafie, A., Pop, I., Non-Darcian effects on natural convection heat transfer in a wavy porous enclosure, *Int. J. Heat Mass Transfer*, *52* (2009), 7-8, pp. 1887-1896.

[3] Choi, S.U.S., Enhancing thermal conductivity of fluids with nanoparticles, *Proceedings* (D.A.Siginer, H.P.Wang), Development and Applications of Non-Newtonian Flows, ASME FED, 1995, Vol.231/MD, Vol. 66, pp. 99-105.

[4] Masuda, H., Ebata, A., Teramae, K., Hishinuma, N., Alteration of thermal conductivity and viscosity of liquid by dispersing ultra fine particles, *Netsu Bussei, 7* (1993), pp. 227-233.
[5] Buongiorno, J., Convective transport in nanofluids, *ASME J. Heat Transfer, 128* (2006), pp. 240-250.
[6] Nield, D.A., Bejan, A., *Convection in Porous Media* (4th edition), Springer, New York, 2013.
[7] Ingham, D.B., Pop, I., *Transport Phenomena in Porous Media*, Vol. III, Elsevier, Oxford, 2005.
[8] Vafai K., *Porous Media: Applications in Biological Systems and Biotechnology*, CRC Press, Tokyo 2010.
[9] Pop, I., Ingham, D.B., *Convective Heat Transfer: Mathematical and Computational Modeling of Viscous Fluids and Porous Media*, Pergamon, Oxford, 2001.
[10] Akbar, N.S., Nadeem, S., Haq, R.U., Khan, Z.H., Radiation effects on MHD stagnation point flow of nano fluid towards a stretching surface with convective boundary condition, *Chinese Journal of Aeronautics, 26* (2013), 6, pp. 1389-1397.
[11] Akbar, N.S., Nadeem, S., Haq, R.U., Khan, Z.H., Numerical solutions of magnetohydrodynamic boundary layer flow of tangent hyperbolic fluid towards a stretching sheet, *Indian Journal of Physics, 87* (2013), 11, pp. 1121-1124.
[12] Akbar, N.S., Khan, Z.H., Nadeem, S., The combined effects of slip and convective boundary conditions on stagnation-point flow of CNT suspended nanofluid over a stretching sheet, *Journal of Molecular Liquids, 196* (2014), pp. 21-25.
[13] Akbar, N.S., Double-diffusive natural convective peristaltic flow of a Jeffrey nanofluid in a porous channel, *Heat Transfer Research, 45* (2014), 4, pp. 293-307.
[14] Akbar, N.S., Peristaltic Sisko nano fluid in an asymmetric channel, *Applied Nanoscience, 4* (2014), 6, pp. 663-673.
[15] Vadasz, P., Heat conduction in nanofluid suspensions, *ASME J. Heat Transfer, 128* (2006), pp. 465-477.
[16] Sheremet, M.A., Pop, I., Natural convection in a square porous cavity with sinusoidal temperature distributions on both side walls filled with a nanofluid: Buongiorno's mathematical model, *Transport in Porous Media, 105* (2014), pp. 411-429.
[17] Sheremet, M.A., Pop, I., Natural convection in a wavy porous cavity with sinusoidal temperature distributions on both side walls filled with a nanofluid: Buongiorno's mathematical model, *ASME J. Heat Transfer, 137* (2015), 072601.
[18] Nield, D.A., Kuznetsov, A.V., Thermal instability in a porous medium layer saturated by a nanofluid: A revised model, *Int. J. Heat Mass Transfer, 68* (2014), pp. 211-214.
[19] Deng, Q.-H., Chang, J.-J., Natural convection in a rectagular enclosure with sinusoidal temperature distributions on both side walls, *Numer. Heat Transfer, Part A, 54* (2008), 5, pp. 507-524.
[20] Oztop, H.F., Abu-Nada, E., Varol, Y., Chamkha, A., Natural convection in wavy enclosures with volumetric heat sources, *Int. J. Thermal Sciences, 50* (2011), 4, pp. 502-514.
[21] Sheremet, M.A., Grosan, T., Pop, I., Free convection in shallow and slender porous cavities filled by a nanofluid using Buongiorno's model, *ASME J. Heat Transfer, 136* (2014), 082501.
[22] Sheremet, M.A., Pop, I., Conjugate natural convection in a square porous cavity filled by a nanofluid using Buongiorno's mathematical model, *Int. J. Heat Mass Transfer, 79* (2014), pp. 137-145.